frontiers in Materials

ORIGINAL RESEARCH
published: 20 December 2021
doi: 10.3389/fmats.2021.767179

Effect of Galvanic Corrosion on the Degradability of Biomedical Magnesium

Hongzhou Peng[1†], Wei Wang[2†], Haomiao Jiang[1], Rui Zan[1], Yu Sun[1], Song Yu[2], Jiahua Ni[3], Wenhui Wang[1], Tao Wang[4]*, Jian Wang[2]* and Xiaonong Zhang[1,5]**

[1]State Key Laboratory of Metal Matrix Composites, School of Materials Science and Engineering, Shanghai Jiao Tong University, Shanghai, China, [2]Department of Hepatobiliary and Pancreatic Surgery, Shanghai Jiao Tong University Affiliated Sixth People's Hospital, Shanghai, China, [3]Department of Mechanical Engineering, Massachusetts Institute of Technology, Cambridge, MA, United States, [4]Department of Orthopaedics and Traumatolog, Shanghai East Hospital, School of Medicine, Tongji University, Shanghai, China, [5]Suzhou Origin Medical Technology Co. Ltd., Suzhou, China

OPEN ACCESS

Edited by:
Changjiang Pan,
Huaiyin Institute of Technology, China

Reviewed by:
Sara Ferraris,
Politecnico di Torino, Italy
Shokouh Attarilar,
Shanghai Jiao Tong University, China
Feng Wu,
Xuzhou University of Technology, China

***Correspondence:**
Xiaonong Zhang
xnzhang@sjtu.edu.cn
Jian Wang
dr_wangjian@126.com
Tao Wang
happywt0403@126.com
Wenhui Wang
wenhuiwang@sjtu.edu.cn

[†]These authors have contributed equally to this work

Specialty section:
This article was submitted to Biomaterials, a section of the journal Frontiers in Materials

Received: 30 August 2021
Accepted: 19 November 2021
Published: 20 December 2021

Citation:
Peng H, Wang W, Jiang H, Zan R, Sun Y, Yu S, Ni J, Wang W, Wang T, Wang J and Zhang X (2021) Effect of Galvanic Corrosion on the Degradability of Biomedical Magnesium. Front. Mater. 8:767179. doi: 10.3389/fmats.2021.767179

With recent progress in clinical trials and scale-up applications of biodegradable magnesium-based implants, the scenarios of transplanting biodegradable Mg with other non-degradable metals may occur inevitably. Galvanic corrosion appears between two metallic implants with different electrochemical potentials and leads to accelerated degradation. However, a quantitative measurement on the galvanic corrosion of Mg in contact with other metallic implants has not been conducted. Here we study the corrosion behaviors and mechanical attenuation of high purity magnesium (Mg)in contact with stainless steel (316L), pure titanium (TA2), and magnesium alloy (AZ91) respectively to form different galvanic couples in simulated body fluids. The results show that all of these three heterogeneous metal pairs accelerate the degradation of high purity Mg to different degrees, yielding declined tensile strength and mechanical failure after 4 days of immersion. Our observations alert the potential risk of co-implanting different metallic devices in clinical trials.

Keywords: biomedical materials, magnesium, galvanic corrosion, mechanical property, degradable metal

INTRODUCTION

In clinical practice, different metallic biomaterials were often used for implantation to achieve specific therapeutic effects (Rostoker et al., 1978; Gilbert et al., 1993; Reclaru and Meyer, 1994). However, these different metal materials with different free corrosion potential are likely to undergo galvanic corrosion after co-implantation. Mathiesen et al. (1991) first observed that the surfaces of the cobalt-chromium alloy and the titanium alloy taken out from the patient's body had obvious galvanic corrosion signs. In dentistry, the galvanic current between the amalgam and other metal restorations is affected by the restoration age and the total surface area (Sutow et al., 2004). Besides, some studies have clearly pointed out that the co-implantation of stainless steel implants with other metallic implants (e.g., pure titanium, titanium alloy, and cobalt alloy) should be avoided in clinical practice (Koh et al., 2015).

Magnesium and its alloys have become attractive degradable materials due to their excellent biocompatibility, mechanical properties, and biodegradability (Staiger et al., 2006; Zhang et al., 2010; Zheng et al., 2014). Some representative degradable and absorbent magnesium alloy implant device products have gradually entered clinical trials and practical applications (Haude et al., 2013; Windhagen et al., 2013; Sun et al., 2019). In recent years, more and more cases of magnesium

co-implantation with other metals have been reported. Hou et al. (Hou et al., 2017) implanted magnesium nails and titanium nails into the femur of SD rats at intervals of 5 and 10 mm and found the sign of increased corrosion. Tian et al. (Tian et al., 2018) developed an innovative magnesium/titanium hybrid system for fixation of bone fracture. Experimental results show that the fixation system can provide sufficient mechanical support for the fracture site while promoting fracture healing. However, magnesium and its alloys have low corrosion potential with high corrosion rate. Galvanic corrosion will occur after magnesium metal devices contact with other metal devices, which accelerates the degradation rate of magnesium, and causes magnesium metal devices to fail during the entire implantation cycle due to accelerated mechanical attenuation. In addition, many studies have proved that magnesium degradation products have certain biological effects on surrounding cells and tissues (Peng et al., 2021; Zan et al., 2021). However, due to the accelerated corrosion of magnesium metal devices, the high concentration of local corrosion products and high local alkalinity are more likely to cause tissue necrosis (Song, 2007). Besides, the degradation process may also release degraded particles that have a negative impact on the tissues (Attarilar et al., 2020; Jin et al., 2020). This is a key scientific issue related to the successful implantation of medical magnesium devices in clinical applications.

At present, the influence of galvanic corrosion on magnesium corrosion behavior has been reported in the industry (Song et al., 2004; Coy et al., 2010), but the employed corrosion environment is usually NaCl solution or salt spray environment, which is different from the biomedical environment. Alloying elements, surface treatment, processing, and other factors can be successfully reflected in the corrosion test in NaCl solution, but other components in the internal environment, such as carbonate, phosphate, and calcium ions, will seriously affect the corrosion rate and corrosion mechanism of magnesium (Xin et al., 2008; Zeng et al., 2014; Mei et al., 2020). In the research of biomedical magnesium corrosion, the choice of corrosive media is one of the important contents of the test. More and more complex media have been used in the corrosion detection of biomedical magnesium. The influence of galvanic action on the corrosion behavior and corrosion mechanical attenuation of medical magnesium remains to be explored in the biomedical environment. Therefore, in this paper, the co-implantation of Mg with other typical biomedical metals during the *in vitro* degradation process were studied to reveal the effect of galvanic corrosion on the degradation properties of Mg, including corrosion behavior and mechanical attenuation. Three different heterogeneous metals (316L stainless steel, TA2 pure titanium, and AZ91 magnesium alloy) relate to high-purity magnesium samples in PBS solution, which is a widely used corrosion medium for testing the biomedical applicability of magnesium, to form a galvanic pair. The corrosion behavior of high-purity magnesium under the effect of galvanic couples was studied through the *in vitro* immersion test, and the attenuation of its mechanical properties was quantified. Our research provided risk hints for the clinical application of magnesium-based medical devices when co-implanted with other metals.

EXPERIMENTAL METHODS

Material Preparation

The experimental samples used in this study were prepared from four metal plates including high purity magnesium (99.98%), magnesium alloy AZ91, pure titanium TA2, and stainless steel 316L (provided by Suzhou Origin Medical Technology Co., Ltd). The composition of the pure magnesium ingot was shown in **Table 1**. The high-purity magnesium plate was processed into tensile specimens. The other three metal plates were cut into thin slices, the size of which (18 × 3.5 × 1.5 mm) was the same as that of the parallel part of the high-purity magnesium tensile specimen.

Electrochemical Test

The various metal pieces were used as working electrodes, which were placed in the solution with an exposed surface of 1 cm^2. The saturated calomel electrode and the platinum electrode were respectively used as the reference electrode and the counter electrode to form a three-electrode system. An electrochemical workstation (CHI660E) was used to measure the open circuit voltage (OCP) of the four metal sheets in 200 ml of PBS solution, and the duration time was 600s.

In Vitro Immersion Test

The high-purity magnesium specimen was separately tied with AZ91, TA2, 316L and immersed in 100 ml PBS solution at 37 ± 0.5°C. The chuck part of the tensile specimen was isolated from the solution, and only the parallel part was in contact with the solution. Immersion tests were suspended in PBS for different time points, t = 12, 24, 48, and 96 h.

After the samples were taken out of the solution, chromic acid solution (prepared as reference (Chen et al., 2020)) was used to remove corrosion products. SEM (FEI Sirion200) was used to characterize the corrosion morphology. After the samples were weighed after corrosion, the corrosion rate was calculated according to the following formula:

$$CR = \frac{K \times W}{A \times T \times D} \quad (1)$$

Where K was a constant (8.76×10^4), W was the weight loss (g), A was the exposed area of the sample in the solution (cm^2), T was the immersion time (h), and D was the material density (for magnesium, the value is 1.74g/cm^3) (Wu et al., 2019).

Mechanical Performance Test and Fracture Topography Analysis

The tensile test was carried out at room temperature using an ETM1048 tensile testing machine with a displacement rate of 2 mm/min, and the morphology of the tensile fracture was

TABLE 1 | Chemical compositions of high-purity magnesium plates.

Element	Al	Si	Mn	Fe	Zn	Ti	Ni	Mg
wt./%	0.001	0.002	0.002	0.002	0.002	<0.001	<0.0005	Balance

TABLE 2 | Electrochemical property data of 4 kinds of metals in PBS.

Metal	Mg	AZ91	TA2	316L
E_c/V	−1.90	−1.67	−0.40	−0.20

observed with the scanning electron microscope (SEM) (FEI Sirion200).

EXPERIMENTAL RESULTS AND ANALYSIS

Corrosion Products and Corrosion Rate

The order of the corrosion potential (E_c) of the four metals in the PBS solution was Mg < AZ91 < TA2 <316L and the specific values are shown in **Table 2**. The macroscopic corrosion morphology of each group of high-purity magnesium plates was shown in **Figure 1**. It could be found that under the influence of three different heterogeneous metal sheets, the corrosion of magnesium was more severe. The weight loss and corrosion rate of each group were shown in **Figure 2**. The acceleration of corrosion was more obvious. During the 96 h immersion process, the weight loss and corrosion rate of high-purity magnesium plates connected with the metal plates were significantly higher than those of the unpaired Mg group. At the same time, during the entire immersion test, the corrosion rate of the Mg group was relatively stable. In the other three groups with galvanic pairing, the average corrosion rate in 96 h was significantly lower than the corrosion rate in the first 12 h, and the overall average corrosion rate showed a significant downward trend.

After 96 h of immersion in each group of high-purity magnesium samples, the surface morphology and the chemical composition of the corrosion products were shown in **Figure 3** characterized by SEM with EDS. It could be seen that there was less deposition of corrosion products on the surface of the Mg group, and a flaky corrosion product layer with cracks covered the surface. The EDS results showed that the composition was mainly composed of three elements: Mg, O, and P, and the atomic ratio of P to Mg was 0.39.

In the other three groups, the inhomogeneous and porous corrosion product layer still existed, but the difference in the thickness of the corrosion product layer was significantly higher than that of the Mg group. Besides, it could be found that a columnar corrosion product accumulated on the product layer. Among them, the uneven degree of corrosion product layer and the accumulation of columnar corrosion product layer in the Mg&316L group were the most serious, and the surface was almost completely covered by such kind of product, while such phenomenon was the least obvious in the Mg&AZ91 group. EDS mapping showed that the element composition on the surface of the sample was still O, Mg, P three elements, but the proportions were not the same. The P/Mg in the Mg&AZ91 group was 0.48, the Mg&TA2 group was 0.67, and the Mg&316L group was 0.96, showing an increasing trend. At the same time, the chemical elements were performed on the columnar sediments. The results showed that the element composition of the three groups were relatively similar, and the P element accounted for a relatively high proportion.

The galvanic corrosion rate was mainly determined by the open circuit potential of the galvanic pair, the resistance of the cathode, the resistance of the anode, and the resistance between the anode and the cathode (Song, 2005). In this study, the corrosion rate of high-purity magnesium samples in the three groups with galvanic couples was positively correlated with the order of the open circuit potential. This was in line with the theory of galvanic corrosion. The peak of the average corrosion rate appears in the first 12 h, and the corrosion rate showed a significant downward trend, but the corrosion rate of the Mg group remained almost constant, which might be determined by the corrosion behavior of magnesium in the PBS solution.

The degradation behavior of magnesium in PBS solution was divided into two aspects: the corrosion of magnesium and the

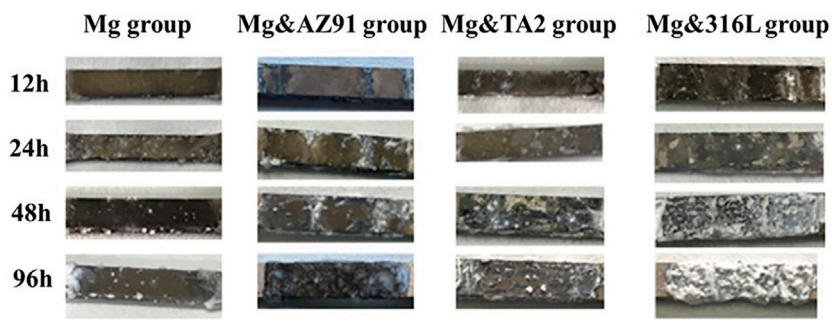

FIGURE 1 | Macroscopic corrosion morphology of magnesium surface under different corrosion conditions.

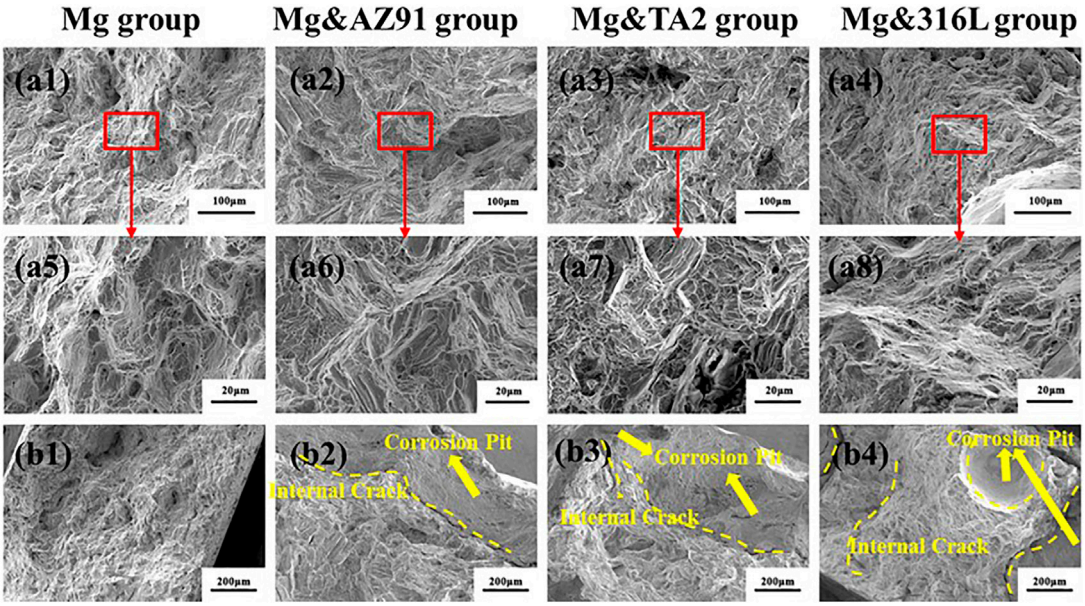

FIGURE 2 | (A) Weight loss of magnesium under different corrosion conditions in PBS solution; **(B)** Corrosion rate of magnesium under different corrosion conditions in PBS solution.

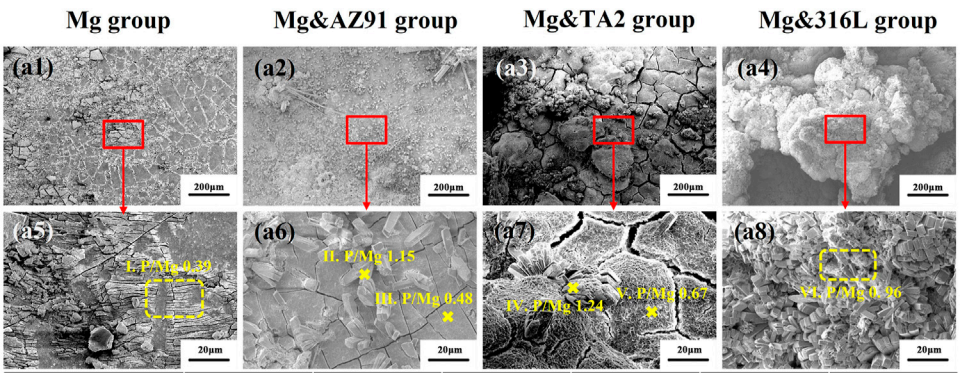

Elements / at.%	Group I	Group II	Group III	Group IV	Group V	Group VI
Mg	31.94	14.45	23.35	13.13	17.04	15.86
P	12.31	16.61	11.32	16.31	11.43	15.15
O	55.76	68.94	65.33	70.56	71.52	69
P/Mg	0.39	1.15	0.48	1.24	0.67	0.96

FIGURE 3 | Surface morphologies with corrosion products and EDS results of HP-Mg in Mg group (b1, b5), Mg&AZ91 group (b2, b6), Mg&TA2 group (b3, b7), and Mg&316L group (b4, b8) after 96 h

deposition of corrosion products on the surface of magnesium. Hydrogen evolution corrosion of magnesium produces OH^-, which formed a corrosion product layer of $Mg(OH)_2$ on the surface of magnesium. In the solution, $Mg(OH)_2$ could combine with water molecules to form hydrates. After the solution was taken out and air-dried, many cracks were formed on the surface of $Mg(OH)_2$, which was shown in **Figures 3b1, b5**. When galvanic corrosion was triggered, the corrosion would increase and the OH^- concentration on the magnesium surface would greatly increase. The hydrogen phosphate and dihydrogen phosphate ions in the solution were likely to react as follows:

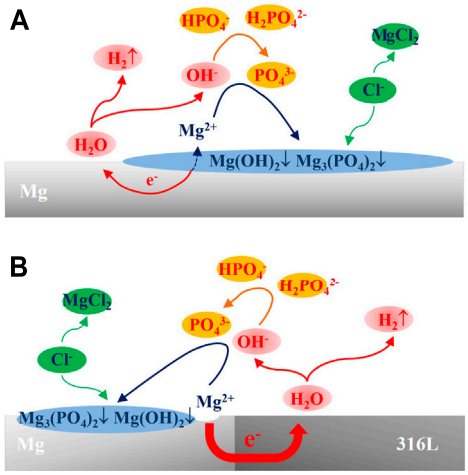

C

$$Mg + e^- \rightarrow Mg^{2+}$$

$$H_2O + e^- \rightarrow OH^- + H_2\uparrow$$

$$Mg^{2+} + OH^- \rightarrow Mg(OH)_2\downarrow$$

$$Mg(OH)_2 + Cl^- \rightarrow MgCl_2 + OH^-$$

$$H_2PO_4^- / HPO_4^{2-} + OH^- \rightarrow PO_4^{3-} + H_2O$$

$$Mg^{2+} + PO_4^{3-} \rightarrow Mg_3(PO_4)_2\downarrow$$

FIGURE 4 | Corrosion mechanism of magnesium in PBS solution: **(A)** Self-corrosion mechanism of magnesium in PBS solution; **(B)** Galvanic corrosion mechanism of magnesium in PBS solution; **(C)** Chemical reaction of magnesium during corrosion process in PBS solution.

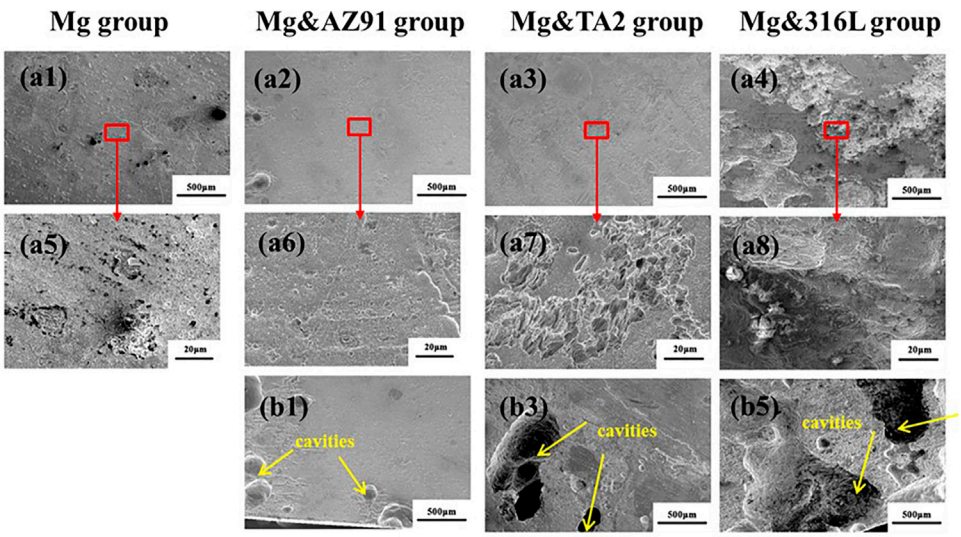

FIGURE 5 | Morphologies of typical corrosion **(A)** and severe pitting corrosion **(B)** of Mg in Mg group (a1, a5), Mg&AZ91 group (a2, a6, b1), Mg&TA2 group (a3, a7, b2) and Mg&316L group (a4, a8, b3) after 96 h

$$H_2PO_4^- + 2OH^- \rightarrow PO_4^{3-} + 2H_2O \quad (2)$$

$$HPO_4^{2-} + OH^- \rightarrow PO_4^{3-} + H_2O \quad (3)$$

Previous studies (Morks, 2004) have shown that magnesium dihydrogen phosphate could directly generate stable magnesium phosphate corrosion products through the following reaction:

$$3Mg(H_2PO_4)_2 + 4H_2O \rightarrow Mg_3(PO_4)_2 \cdot 4H_2O + 4H_3PO_4 \quad (4)$$

Since the solubility product constant K_{sp} of $Mg_3(PO4)_2$ at room temperature was 1.04×10^{-24}, which was much smaller than 1.8×10^{-11} of $Mg(OH)_2$, magnesium ions tended to form more stable magnesium phosphate. It was reflected in the white columnar products with high phosphorus content in **Figures 3b2–b4, b6–b8**. The more significant the galvanic corrosion and the more OH^- released, causing a denser product layer, which was reflected in the higher the phosphorus content of the product layer. The accumulation of this magnesium-containing phosphate corrosion product layer could reduce the corrosion rate of the magnesium matrix (Xu et al., 2008) so that the corrosion rate of magnesium under the action of the galvanic pair was significantly reduced. Besides, the accumulation of non-conductive corrosion product layers could reduce the effect of galvanic corrosion by increasing the resistance between the anode and the cathode. **Figure 4** summarized the degradation

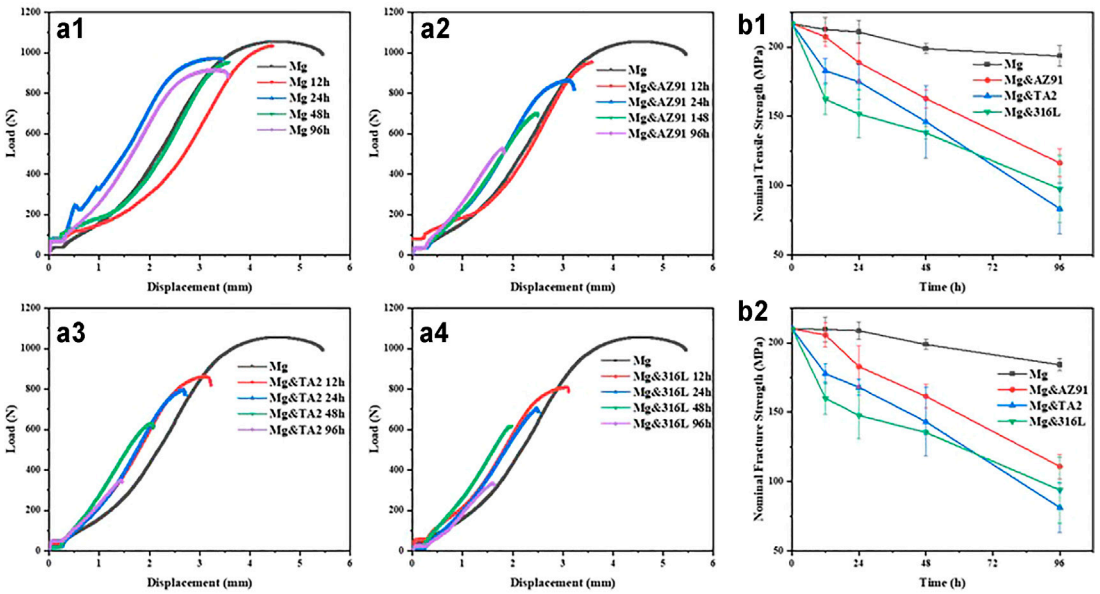

FIGURE 6 | Load-displacement curve of HP-Mg in Mg group (a1), Mg&AZ91 group (a2), Mg&TA2 group (a3) and Mg&316L group (a4), nominal tensile strength (b1) and nominal fracture strength (b2) of Mg after corrosion.

mechanism of galvanically corroded magnesium and self-corrosive magnesium in PBS solution.

Corrosion Morphology

Figure 5 showed the SEM image of the corrosion products morphology of the four groups of samples after cleaning. In the three groups of samples with galvanic couples, most of the areas were similar to the Mg group, showing the morphology of corroded micropores, but the corroded pores were deeper and more obvious in comparison. Besides, there were areas of severe pitting corrosion in the three groups, which mostly appeared on the edges of the samples, and large and deep cavities were formed. Such a phenomenon was not found in the Mg group. the area where the galvanic current of the magnesium alloy acts was limited and the galvanic current was unevenly distributed. In the area where the galvanic current density was relatively large, the rate of anode dissolution was accelerated, and the overpotential value of anode dissolution increased, which caused the electrode reaction to deviate from equilibrium and the generation of magnesium ions increased. In order to maintain the neutrality of the solution, anions would migrate to the anode area, which included Cl^- ions. Cl^- could corrode the corrosion product film layer and cause pitting corrosion through the reaction below (Song and Atrens, 1999; Esmaily et al., 2017):

$$Mg(OH)_2 + 2Cl^- \rightarrow Mg^{2+} + 2OH^- \quad (5)$$

Attenuation of Mechanical Properties and Fracture Analysis

In this study, the nominal tensile strength and nominal fracture strength were used to characterize the mechanical properties of the high-purity magnesium specimens after corrosion. The maximum tensile strength and the breaking force were divided by the initial cross-sectional area of the sample before being corroded. As shown in **Figures 6a1–a4**, after 96 h of soaking, the nominal tensile strength of the Mg group, Mg&AZ91 group, Mg&TA2 group, and Mg&316L group decreased from 216.89 MPa to 193.50, 116.43, 83.44, and 97.67 MPa respectively, while the fracture strength attenuated from 210.24 MPa to 184.20, 110.86, 81.23, and 93.81MPa, respectively. The shapes of the load-displacement curves of all groups were similar and there was no obvious yield step found. The mechanical properties were gradually reduced with the passage of corrosion time, and the degree of attenuation was positively correlated with the severity of corrosion, except for the abnormal results between Mg&TA2 group and Mg&316L group immersed for 96 h.

Figure 7 showd the fracture morphology of each group of Mg samples after corrosion for 96 h. The morphology of the fracture center (**Figure 7A**) that was not affected by corrosion was relatively similar and was relatively flat macroscopically. At high magnification, its morphology was a mixed fracture composed of small cleavage facets, dimples, and tearing edges, showing typical quasi-cleavage fracture characteristics. However, the morphology of the edge of the fracture (**Figure 7B**) showed that the fracture surface of the Mg group was still relatively neat, but the fracture morphology of the center and the edge of the three groups of Mg tensile specimens with galvanic pairing was significantly different. In these three groups, the fracture cross-section reflected in the fracture macro morphology was already very irregular, and there were long and deep internal cracks at the same time.

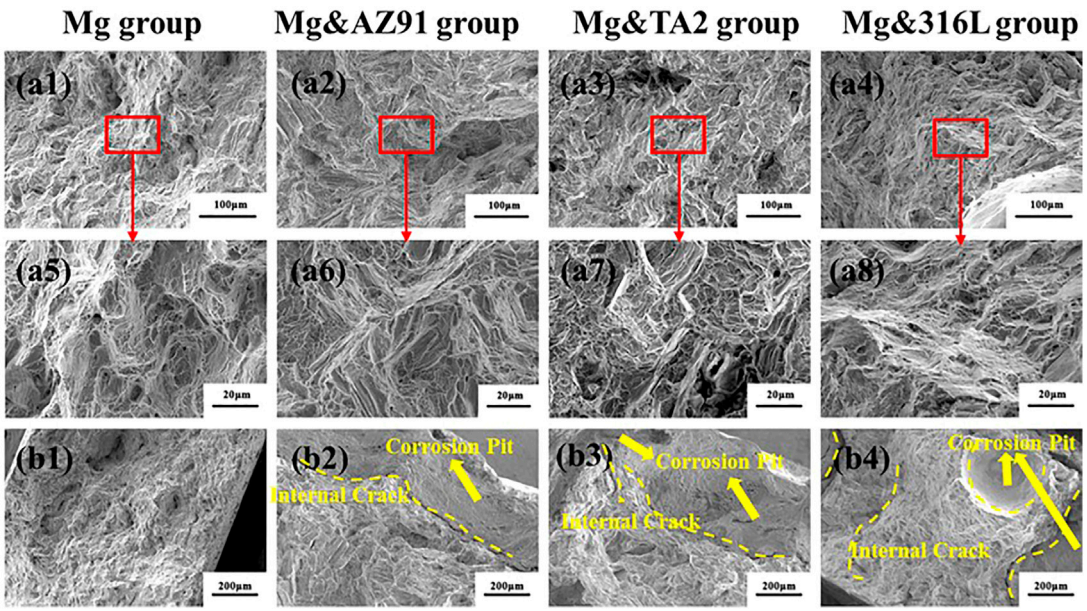

FIGURE 7 | The fracture images of Mg from center **(A)** to edge **(B)** in Mg group (a1, a5, b1), Mg&AZ91 group (a2, a6, b2), Mg&TA2 group (a3, a7, b3) and Mg&316L group (a4, a8, b4) after 4d

The calculation method of the nominal mechanical properties determines that weight loss became a cause of mechanical attenuation in this study. Assuming that all Mg samples were completely uniformly corroded in each phase during corrosion, corrosion only caused the Mg samples to keep the original shape and shrank proportionally, without causing stress concentration. Under this hypothetical ideal test condition, for the sample with the highest weight loss (soaked with 316L for 96 h), its weight loss rate was 24.7%, but the attenuation of its nominal tensile strength far exceeds this, reaching 55.0%. Therefore, in the actual immersion corrosion situation, a large part of the attenuation of mechanical properties was not caused by weight loss.

Due to the limited plastic deformation ability of high-purity magnesium at room temperature, the stress-concentrated tip part could not well relieve stress concentration by expanding the load-bearing area through plastic deformation and was extremely sensitive to stress concentration and crack size. The testing results of each group showed that as the corrosion intensified, the total length of the tensile curve gradually became shorter, and the tensile strength gradually decreased, reflecting a certain extent the reduction in the deformability and nominal fracture strength of Mg as the corrosion intensified. However, at the same time, the fracture morphology at the center that was not affected by corrosion also shows that the matrix of the Mg sample had no significant change. This was mainly due to the formation of corrosion pits on the surface. The size of corrosion pits was usually much larger than internal defects, and the impact of surface perforation caused by corrosion on the tensile strength of magnesium alloys was more serious than internal defects (Wang et al., 2010). Because the corrosion pits made the geometrical surface of the sample more irregular and the curvature became larger, the stress concentration was more likely to occur when such defects were under tensile stress. Therefore, the microcracks were more likely to nucleate and gather in the corrosion pits, and were more likely to be localized it spreads around, forming cracks and causing fracture. Studies had pointed out that the depth of pits was closely related to the residual strength of magnesium alloys after corrosion (Li et al., 2010). When the corrosion pit gradually deepened, the stress concentration intensifies, and internal cracks began to occur, which further intensifies the crack propagation. For samples with severe corrosion, pits gather on the surface and increase in size, resulting in serious stress concentration in these parts, and the fractures directly showed the shape of the edges of the pits.

CONCLUSION

1) High-purity magnesium is connected to three heterogeneous metals (316L, TA2, AZ91). After being immersed in PBS solution, different degrees of galvanic corrosion are produced, and the degree of acceleration is positively correlated with the potential difference of each galvanic pair.
2) The generation of galvanic corrosion, on the one hand, leads to more deposition of phosphate corrosion products by causing the accelerated release of OH^-, which could protect the magnesium matrix. This makes the average corrosion rate of high-purity magnesium decrease more obviously after 24 h immersion. In the long run, the presence of phosphate will significantly inhibit the

galvanic corrosion of high-purity magnesium. On the other hand, large and deep pits were observed since galvanic corrosion caused significant local corrosion, which may be caused by the accumulation of anions on the sample surface under the uneven current of the galvanic.

3) The tensile strength of magnesium decreased significantly in the presence of the galvanic couple, and the tensile strength reached 60% after 96 h of co-immersion. This is probably caused by the deep pitting corrosion mentioned in conclusion (2). The risk that this huge mechanical attenuation requires close attention in the clinic.

DATA AVAILABILITY STATEMENT

The original contributions presented in the study are included in the article/supplementary material, further inquiries can be directed to the corresponding authors.

AUTHOR CONTRIBUTIONS

XZ, JW, TW, and WW contributed to conception and design of the study. HP, WW, and SY organized the database. WW, RZ, JN, and HP performed the statistical analysis. HP and HJ wrote the first draft of the manuscript. HP, HJ, and WW wrote sections of the manuscript. All authors contributed to manuscript revision, read, and approved the submitted version.

FUNDING

This work was financially supported by the Science and technology commission of Shanghai Municipality (No.19441905600), the Shanghai Jiao Tong University Interdisciplinary (Biomedical Engineering) Research Fund (No. ZH2018ZDA09), Three-Year Initiative Plan for Strengthening Public Health System Construction in Shanghai (GWV-10.1-XK21).

REFERENCES

Attarilar, S., Yang, J., Ebrahimi, M., Wang, Q., Liu, J., Tang, Y., et al. (2020). The Toxicity Phenomenon and the Related Occurrence in Metal and Metal Oxide Nanoparticles: A Brief Review from the Biomedical Perspective. *Front. Bioeng. Biotechnol.* 8, 822. doi:10.3389/fbioe.2020.00822

Chen, B., Wu, H., Yi, R., Wang, W., Xu, H., Zhang, S., et al. (2020). *In Vitro* crevice Corrosion of Biodegradable Magnesium in Different Solutions. *J. Mater. Sci. Techn.* 52, 83–88. doi:10.1016/j.jmst.2020.04.014

Coy, A. E., Viejo, F., Skeldon, P., and Thompson, G. E. (2010). Susceptibility of Rare-Earth-Magnesium Alloys to Micro-galvanic Corrosion. *Corrosion Sci.* 52, 3896–3906. doi:10.1016/j.corsci.2010.08.006

Esmaily, M., Svensson, J. E., Fajardo, S., Birbilis, N., Frankel, G. S., Virtanen, S., et al. (2017). Fundamentals and Advances in Magnesium alloy Corrosion. *Prog. Mater. Sci.* 89, 92–193. doi:10.1016/j.pmatsci.2017.04.011

Gilbert, J. L., Buckley, C. A., and Jacobs, J. J. (1993). *In Vivo* corrosion of Modular Hip Prosthesis Components in Mixed and Similar Metal Combinations. The Effect of Crevice, Stress, Motion, and alloy Coupling. *J. Biomed. Mater. Res.* 27, 1533–1544. doi:10.1002/jbm.820271210

Haude, M., Erbel, R., Erne, P., Verheye, S., Degen, H., Böse, D., et al. (2013). Safety and Performance of the Drug-Eluting Absorbable Metal Scaffold (DREAMS) in Patients with De-novo Coronary Lesions: 12 Month Results of the Prospective, Multicentre, First-In-Man BIOSOLVE-I Trial. *The Lancet* 381, 836–844. doi:10.1016/s0140-6736(12)61765-6

Hou, P., Han, P., Zhao, C., Wu, H., Ni, J., Zhang, S., et al. (2017). Accelerating Corrosion of Pure Magnesium Co-implanted with Titanium *In Vivo*. *Sci. Rep.* 7, 41924. doi:10.1038/srep41924

Jin, L., Chen, C., Jia, G., Li, Y., Zhang, J., Huang, H., et al. (2020). The Bioeffects of Degradable Products Derived from a Biodegradable Mg-Based alloy in Macrophages via Heterophagy. *Acta Biomater.* 106, 428–438. doi:10.1016/j.actbio.2020.02.002

Koh, J., Berger, A., and Benhaim, P. (2015). An Overview of Internal Fixation Implant Metallurgy and Galvanic Corrosion Effects. *J. Hand Surg.* 40, 1703–1710. e4. doi:10.1016/j.jhsa.2015.03.030

Li, C., Liu, Y., Wang, Q., Zhang, L., and Zhang, D. (2010). Study on the Corrosion Residual Strength of the 1.0wt.% Ce Modified AZ91 Magnesium alloy. *Mater. Characterization* 61, 123–127. doi:10.1016/j.matchar.2009.09.014

Mathiesen, E., Lindgren, J., Blomgren, G., and Reinholt, F. (1991). Corrosion of Modular Hip Prostheses. *The J. Bone Jt. Surg. Br. volume* 73-B, 569–575. doi:10.1302/0301-620x.73b4.2071637

Mei, D., Lamaka, S. V., Lu, X., and Zheludkevich, M. L. (2020). Selecting Medium for Corrosion Testing of Bioabsorbable Magnesium and Other Metals - A Critical Review. *Corrosion Sci.* 171, 108722. doi:10.1016/j.corsci.2020.108722

Morks, M. F. (2004). Magnesium Phosphate Treatment for Steel. *Mater. Lett.* 58, 3316–3319. doi:10.1016/j.matlet.2004.06.027

Peng, H., Fan, K., Zan, R., Gong, Z.-J., Sun, W., Sun, Y., et al. (2021). Degradable Magnesium Implants Inhibit Gallbladder Cancer. *Acta Biomater.* 128, 514–522. doi:10.1016/j.actbio.2021.04.051

Reclaru, L., and Meyer, J.-M. (1994). Study of Corrosion between a Titanium Implant and Dental Alloys. *J. Dentistry* 22, 159–168. doi:10.1016/0300-5712(94)90200-3

Rostoker, W., Galante, J. O., and Lereim, P. (1978). Evaluation of Couple/crevice Corrosion by Prosthetic Alloys Underin Vivo Conditions. *J. Biomed. Mater. Res.* 12, 823–829. doi:10.1002/jbm.820120605

Song, G. (2007). Control of Biodegradation of Biocompatable Magnesium Alloys. *Corrosion Sci.* 49, 1696–1701. doi:10.1016/j.corsci.2007.01.001

Song, G., Johannesson, B., Hapugoda, S., and StJohn, D. (2004). Galvanic Corrosion of Magnesium alloy AZ91D in Contact with an Aluminium alloy, Steel and Zinc. *Corrosion Sci.* 46, 955–977. doi:10.1016/s0010-938x(03)00190-2

Song, G. L., and Atrens, A. (1999). Corrosion Mechanisms of Magnesium Alloys. *Adv. Eng. Mater.* 1, 11–33. doi:10.1002/(sici)1527-2648(199909)1:1<11:aid-adem11>3.0.co;2-n

Song, G. (2005). Recent Progress in Corrosion and Protection of Magnesium Alloys. *Adv. Eng. Mater.* 7, 563–586. doi:10.1002/adem.200500013

Staiger, M. P., Pietak, A. M., Huadmai, J., and Dias, G. (2006). Magnesium and its Alloys as Orthopedic Biomaterials: A Review. *Biomaterials* 27, 1728–1734. doi:10.1016/j.biomaterials.2005.10.003

Sun, Y., Wu, H., Wang, W., Zan, R., Peng, H., Zhang, S., et al. (2019). Translational Status of Biomedical Mg Devices in China. *Bioactive Mater.* 4, 358–365. doi:10.1016/j.bioactmat.2019.11.001

Sutow, E. J., Maillet, W. A., Taylor, J. C., and Hall, G. C. (2004). *In Vivo* galvanic Currents of Intermittently Contacting Dental Amalgam and Other Metallic Restorations. *Dental Mater.* 20, 823–831. doi:10.1016/j.dental.2003.10.012

Tian, L., Sheng, Y., Huang, L., Chow, D. H.-K., Chau, W. H., Tang, N., et al. (2018). An Innovative Mg/Ti Hybrid Fixation System Developed for Fracture Fixation and Healing Enhancement at Load-Bearing Skeletal Site. *Biomaterials* 180, 173–183. doi:10.1016/j.biomaterials.2018.07.018

Wang, Q., Liu, Y. H., Zhang, L. N., Song, Y. L., Zhang, D. W., and Li, C. F. (2010). Study on the Effect of Corrosion on the Tensile Behavior of an AZ91 alloy. *Mater. Corrosion* 61, 222–228. doi:10.1002/maco.200905317

Windhagen, H., Radtke, K., Weizbauer, A., Diekmann, J., Noll, Y., Kreimeyer, U., et al. (2013). Biodegradable Magnesium-Based Screw Clinically Equivalent to Titanium Screw in Hallux Valgus Surgery: Short Term Results of the First Prospective, Randomized, Controlled Clinical Pilot Study. *Biomed. Eng. Online* 12, 62. doi:10.1186/1475-925x-12-62

Wu, H., Zhang, C., Lou, T., Chen, B., Yi, R., Wang, W., et al. (2019). Crevice Corrosion - A Newly Observed Mechanism of Degradation in Biomedical Magnesium. *Acta Biomater.* 98, 152–159. doi:10.1016/j.actbio.2019.06.013

Xin, Y., Huo, K., Tao, H., Tang, G., and Chu, P. K. (2008). Influence of Aggressive Ions on the Degradation Behavior of Biomedical Magnesium alloy in Physiological Environment. *Acta Biomater.* 4, 2008–2015. doi:10.1016/j.actbio.2008.05.014

Xu, L., Zhang, E., Yin, D., Zeng, S., and Yang, K. (2008). *In Vitro* corrosion Behaviour of Mg Alloys in a Phosphate Buffered Solution for Bone Implant Application. *J. Mater. Sci. Mater. Med.* 19, 1017–1025. doi:10.1007/s10856-007-3219-y

Zan, R., Ji, W., Qiao, S., Wu, H., Wang, W., Ji, T., et al. (2021). Biodegradable Magnesium Implants: a Potential Scaffold for Bone Tumor Patients. *Sci. China Mater.* 64 (4), 1007–1020. doi:10.1007/s40843-020-1509-2

Zeng, R.-C., Hu, Y., Guan, S.-K., Cui, H.-Z., and Han, E.-H. (2014). Corrosion of Magnesium alloy AZ31: The Influence of Bicarbonate, Sulphate, Hydrogen Phosphate and Dihydrogen Phosphate Ions in saline Solution. *Corrosion Sci.* 86, 171–182. doi:10.1016/j.corsci.2014.05.006

Zhang, S., Zhang, X., Zhao, C., Li, J., Song, Y., Xie, C., et al. (2010). Research on an Mg-Zn alloy as a Degradable Biomaterial. *Acta Biomater.* 6, 626–640. doi:10.1016/j.actbio.2009.06.028

Zheng, Y. F., Gu, X. N., and Witte, F. (2014). Biodegradable Metals. *Mater. Sci. Eng. R: Rep.* 77, 1–34. doi:10.1016/j.mser.2014.01.001

Conflict of Interest: XZ was employed by Suzhou Origin Medical Technology Co., Ltd.

The remaining authors declare that the research was conducted in the absence of any commercial or financial relationships that could be construed as a potential conflict of interest.

The reviewer SA declared a shared affiliation with several of the authors, HP, WW, HJ, RZ, YS, SY, WW, JW, ZX, to the handling editor at time of review.

Publisher's Note: All claims expressed in this article are solely those of the authors and do not necessarily represent those of their affiliated organizations, or those of the publisher, the editors and the reviewers. Any product that may be evaluated in this article, or claim that may be made by its manufacturer, is not guaranteed or endorsed by the publisher.